AD-780 274

CARBON MONOXIDE LASER

Robert E. Center

Avco Everett Research Laboratory, Incorporated

Prepared for:

Advanced Research Project Agency

May 1974

UNCLASSIFIED
Security Classification

AD 780274

DOCUMENT CONTROL DATA - R & D

(Security classification of title, body of abstract and indexing annotation must be entered when the overall report is classified)

1 ORIGINATING ACTIVITY (Corporate author)	2a. REPORT SECURITY CLASSIFICATION
AVCO EVERETT RESEARCH LABORATORY, INC. 2385 REVERE BEACH PARKWAY EVERETT, MASSACHUSETTS	UNCLASSIFIED
	2b. GROUP

3 REPORT TITLE

CARBON MONOXIDE LASER
ANNUAL TECHNICAL REPORT

4 DESCRIPTIVE NOTES (Type of report and inclusive dates)
Annual Technical Report

5 AUTHOR(S) (First name, middle initial, last name)

Avco Everett Research Laboratory, Inc.

6 REPORT DATE	7a. TOTAL NO OF PAGES	7b. NO. OF REFS
May 1974	48	40

8a. CONTRACT OR GRANT NO	9a. ORIGINATOR'S REPORT NUMBER(S)
N00014-72-C-0030 b. PROJECT NO c. d.	Annual Technical Report 9b. OTHER REPORT NO(S) (Any other numbers that may be assigned this report)

10 DISTRIBUTION STATEMENT

DISTRIBUTION STATEMENT A
Approved for public release;
Distribution Unlimited

11 SUPPLEMENTARY NOTES	12. SPONSORING MILITARY ACTIVITY
	ARPA, DOD, ARPA Order No. 1807, monitored by Code No. 421, ONR, Arlington, Virginia

13 ABSTRACT

The main objective of this program is the investigation of the pulsed electrical CO laser to determine the relevant scaling parameters and the usefulness of high power CO lasers in systems applications. The current contract has included parametric multiline/multimode performance measurements, investigation of the medium homogeneity using interferometric diagnostics, calculations of CO lineshift and linewidth as a function of pressure in CO–N_2 mixtures and detailed parametric performance calculations for both single and multiline operation.

Following the performance measurements of the multiline output as a function of gas mixture, pulse length and applied E/N, considerable time was spent on the medium homogeneity measurements. These measurements, which are described in detail in the semi-annual report, indicated large thermal gradients and turbulence due to the effect of buoyancy forces. Modifications were made to the cavity to minimize these gradients and further lasing performance tests were made as described in the present report. It is concluded that the present cavity flow uniformity is limited by the buoyancy effects to a minimum temperature of approximately – 150°C and a transverse temperature gradient of 0.3°C/cm. It is not feasible to improve the present system beyond this uniformity. It was concluded that a new transverse flow system could be developed to avoid these thermal instability problems.

The parametric performance calculations are described in an appendix to the present report and should prove to be useful for systems design considerations. The calculations have been made for single and multiline outputs as well as selected multiline output. Also included in this report are some detailed lineshift calculations in CO–N_2 mixtures. The shifts are predicted to be less than 0.005 cm^{-1} per atmosphere N_2.

DD FORM 1 NOV 68 1473

UNCLASSIFIED
Security Classification

14 KEY WORDS	LINK A		LINK B		LINK C	
	ROLE	WT	ROLE	WT	ROLE	WT
1. Electric CO Lasers						
2. Multiline Measurements						
3. Medium Homogeneity						
4. Theoretical CO Laser Calculations						
5. Lineshift/Linewidth Calculations						

CARBON MONOXIDE LASER

ANNUAL TECHNICAL REPORT

prepared by

AVCO EVERETT RESEARCH LABORATORY, INC.
a Subsidiary of Avco Corporation
Everett, Massachusetts

May 1974

Contract No. N00014-72-C-0030

supported by

ADVANCED RESEARCH PROJECTS AGENCY
DEPARTMENT OF DEFENSE
ARPA Order No. 1807
monitored by Code No. 421

OFFICE OF NAVAL RESEARCH
Arlington, Virginia

ib

FOREWORD

ARPA Order No.:	1807
Name of Contractor:	Avco Everett Research Laboratory
Effective Data of Contract:	1 November 1971
Contract Expiration Date:	30 December 1973
Amount of Contract:	$498, 257
Contract Number:	N00014-72-C-0030
Principal Investigator and Phone Number:	Dr. Robert E. Center Area Code 617, 389-3000, Ext. 593
Project Scientists:	Dr. M. J. W. Boness G. E. Caledonia Dr. D. Korff
Scientific Officer·	Director, Physics Program Physical Sciences Division Office of Naval Research Department of the Navy Arlington, Virginia 22217
Short Title of Work:	Carbon Monoxide Laser

TABLE OF CONTENTS

LIST OF ILLUSTRATIONS

I. INTRODUCTION

The CO laser program is directed towards the investigation of the performance characteristics of the pulsed electrical CO laser using an electron beam-sustained discharge. The experimental investigation is aimed at evaluating the scaling parameters of high power electrical CO lasers and their potential systems applications. The overall program includes theoretical modeling to provide support for the design of the experiment and the interpretation of the data.

The following areas of investigation were included in the current contract:

1) Parametric investigation of the multiline/multimode performance as a function of gas mixture, pulse length and applied E/N.

2) Measurement of medium homogeneity using an optical interferometer.

3) Investigation of techniques for the efficient extraction of energy on selected transitions.

4) Design and construction of a single mode cavity.

5) Parametric calculations of the pulsed CO lasers for multiline and selected-line operation and comparison of code with experimental data.

6) Calculation of CO lineshift/linewidth in N_2-CO mixtures.

The initial performance measurements and the medium homogeneity tests were described in the previous semi-annual report. These are updated in the present report to take account of the effect of the cavity modifications required to improve the optical qualities of the medium. Although the overall performance has been improved, the measured total electrical efficiency is still a factor of 2 to 3 below the predicted value. This is partly due to the temperature limitations and fluctuations in the present cavity design. Furthermore, some room temperature lasing measurements suggest a significant effect due to (unidentified) impurities. Although a single mode cavity was designed for the present cavity and probe lasers diagnostics built for gain measurements, these studies were delayed by the problems due to the thermal nonuniformities in the cold cavity. It appears necessary to redesign the cavity and flow system in order to reduce the

thermal fluctuations and significantly improve the low temperature performance. A new transverse flow system has been designed which will avoid the buoyancy problems in the present system.

The parametric performance calculations have been made as a function of mixture, temperature, pulse length and electron density for a variety of cavity output conditions including selected line operation. These calculations should be useful in determining criteria for systems designs. The theoretical analyses of lineshift/linewidth in CO-N_2 mixtures has led to predictions of lineshift by N_2 of the order of 0.005 cm^{-1} per atmosphere of N_2 with a broadening width an order of magnitude larger. Such small lineshift suggests the possible application of a MOPA system in a high power CO laser without the necessity of matching the pressure and operating conditions in the oscillator and amplifier.

II. MULTILINE MEASUREMENTS

A. CAVITY MODIFICATIONS

The medium quality was previously examined using a large aperture Mach-Zehnder interferometer aligned parallel to the optical axis of the cavity. The measurement determines the quantity

$$\int \rho \delta \ell$$

which is the integrated optical path parallel to the axis of the cavity. Temperature measurements were performed at a number of stations located upon the cathode surface and in the gas supply manifold. These measurements were performed under cold gas flow conditions without an electrical discharge within the cavity. The diagnostics employed and an analysis of the results obtained were previously described in AERL November 1973 Semi-Annual Report. The results of the measurements indicated considerable disturbances throughout the lasing medium and large thermal gradients over the cathode surface.

Subsequent to these measurements the following modifications were made to both the cavity and to the method of operation.

1) Radiatively shielding the cavity by lining the flow base with aluminum foil.

2) Reducing convective and radiative effects from the E-beam foil by introducing a thin foil between the gun foil and the cathode.

3) The introduction of 60° inclined sidewalls from the edges of the cathode to the sides of the flow box. These walls essentially insulate the medium from the sides of the flow base since th y are foil lined and can be precooled.

4) Introduction of a flow duct above the anode to reduce recirculation through the porous anode.

These modifications are indicated schematically in Fig. 1. Operational modifications included:

1) More efficient use of the flowing gas heat exchanger enabling gas manifold temperatures of $-185^{\circ}C$ to be achieved.

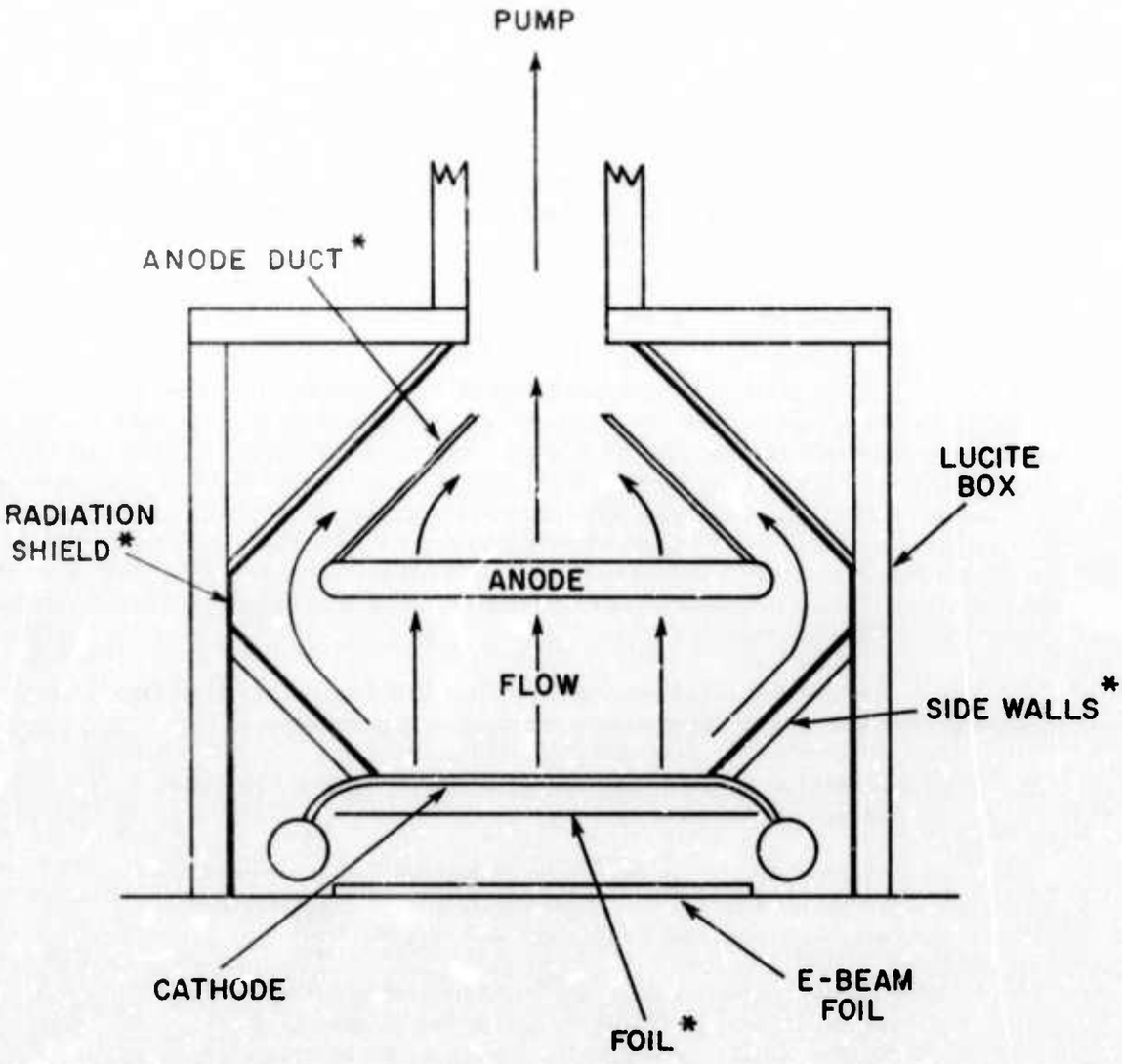

Fig. 1 Schematic of Modified Cavity. Items marked with an asterisk were added to reduce the gas thermal nonuniformities.

2) Elapsed flow times of 2 - 3 minutes were found to significantly reduce turbulent gradients and initial cathode thermal nonuniformities. The final thermal gradients were reduced to approximately $0.2^{\circ}C/cm$ and the transverse gradients to $0.3^{\circ}C/cm$, in addition a reduction of the mean cavity gas temperature by 15 - $20^{\circ}C$ to approximately $-165^{\circ}C$.

Further significant improvements to the temperature uniformity and hence the medium quality are impeded in the present system by the low flow velocity which is limited by the electrode structures and gas handling system.

The compatibility of these cavity modifications with electrical operation of the cavity were investigated over a wide range of operating conditions. As they were originally employed, two of these modifications, namely the 60° inclined sidewalls and the radiation shielding, were found to be incompatible with satisfactory operation of the discharge. Arcing down the sidewalls shown in Fig. 1 was probably associated with a warm thermal boundary layer and was eliminated by reducing the inclination of the sidewalls from 60° to 30° which increased the anode-sidewall spacing.

The aluminum radiation shielding produced intense corona immediately the sustainer voltage was applied. This problem could eventually be overcome by ensuring that none of the foil edges were exposed to the discharge. This task would require complete disassembly of the cavity and may be performed at a later date. The present tests were conducted without radiation shielding on the cavity walls. The foil introduced between the gun foil and the cathode in order to reduce convective and radiative coupling between the gun foil and the medium presented a further impedance to the electron beam. Sustainer current measurements were made both with and without the foil present. No appreciable reduction of the sustainer current was observed. However the foil thickness employed, 1/2 mil Kapton, was unable to consistently withstand the pressure pulse produced by the discharge. A thicker 2 mil foil was tested and successfully withstood the pressure pulse but reduced the sustainer current by 40%. Further efforts are in progress to optimize the foil thickness in terms of these two performance criteria.

B. LOW TEMPERATURE PERFORMANCE

The effect of the cavity modifications upon the output power and electrical efficiency of the laser was examined under cold gas flow and multiline/multimode conditions. Performance measurements were conducted using premixed gases under cold gas flow conditions of nominally $-150^{\circ}C$ and 1/6 atmospheric pressure corresponding to a gas density of one-third Amagat. The somewhat higher gas temperature employed compared with the value of $-165^{\circ}C$ referred to in the previous semi-annual is a consequence of abandoning the radiation shielding on the cavity walls. Theoretical calculations indicate the continuous improvement in lasing

performance achieved by reducing the gas temperature. The design of the new transverse cavity and flow system described in AERLP 379 offers to accomplish substantial reduction in gas temperature.

N_2 and Argon were separately employed as the diluent species in the ratio 80% of diluent to 20% CO. As usual, the gases were passed through an activated alumina filter immersed in dry ice and alcohol before entering the mixing tank. Optimum efficiencies of approximately 20% were obtained for both mixtures. For the N_2-CO mixture this represents an improvement of 5% compared with measurements performed prior to the cavity modifications. Maximum output energies in the region of 1600 joules were obtained for both mixtures. The performance characteristics are summarized in Table I.

Optimal sustainer electric field strengths were 2.5 kV/cm and 1.2 kV/cm comparing N_2 and Ar respectively as the diluent. This variation is attributed to the difference exhibited by the diluents with respect to low energy electron impact processes. Argon substantially increases the electron temperature when employed as the diluent compared with nitrogen. This effect is attributed to the absence of low energy inelastic electron energy loss mechanisms in the case of Ar. Nitrogen on the other hand exhibits very large vibrational excitation cross sections in the region of approximately 2 eV. Argon therefore requires a lower sustainer electric field strength in order to achieve a corresponding electron temperature compared with nitrogen. Further, the low lying energy loss mechanisms exhibited by N_2 efficiently deplete the high energy tail of the electron energy distribution thus raising the sustainer electric field threshold necessary to initiate arcing.

C. ROOM TEMPERATURE OPERATION

Output energy and electrical efficiency were also measured under ambient temperature gas flow conditions. Under these conditions the N_2-CO mixture gave better performance than the Ar-CO mixture; namely optimum efficiency of 6% and 700 joules output compared with 4% efficiency and 200 joules respectively. This difference conceivably indicates that the temperature dependence of the $N_2 \rightarrow CO$ V-V transfer rate is such that under ambient temperature conditions this process contributes to the lasing kinetics. These performance characteristics are summarized in Table 1.

Measurements have also been performed under ambient gas temperature conditions with no gas flow as a function of the residence time of the gas charge in the cavity prior to initiating the discharge. It has been demonstrated that as the residence time increases, both the output energy and the electrical efficiency decrease. This observation suggests that impurities originating from the cavity contaminate the gas mixture. Such impurities may be important in the deactivation of vibrationally excited CO. Outgassing from the cavity walls and components is the most likely source of the contamination since leak detector tests have confirmed the vacuum integrity of the cavity. Attention is being given to the outgassing properties of the materials to be employed in the new flow system.

TABLE I

PERFORMANCE CHARACTERISTICS

Mixture Ratio 80% Diluent : 20% CO

Density = 0.33 Amagat

Temperature (^{o}C)	Diluent	Sustainer Electric Field (kV/cm)	Output (Joules)	Pulse Length (μsecs)	Efficiency %
-150	N_2	2.5	1500	90	20
	Ar	1.3	1720	90	19
20	N_2	3.0	700	80	5.8
	Ar	2.0	200	40	4

APPENDIX A

PARAMETRIC PERFORMANCE CALCULATIONS

A. INTRODUCTION

The electrically excited CO laser has received considerable attention recently because of its demonstrated high operating efficiency.[1, 2] The basic kinetic concepts appropriate to the CO laser have been studied in detail.[3-8] It has been shown that the partial inversions and high efficiency result from vibrational relaxation processes in the anharmonic oscillator, CO, under conditions of thermal nonequilibrium.[3-9] These analyses have been concerned with the understanding of the kinetic processes involved and the development of numerical results for comparison with specific experimental measurements of pulse shape, electrical efficiency and spectral distribution. The basic purpose of the present calculations is to present a comprehensive survey of the dependence of the electrical CO laser performance on parameters such as gas mixture, translational temperature, and the discharge pulse length for both multiline and selective line operations. These calculations are intended to serve as a guide in the design and development of high power electrical CO lasers for a variety of operating conditions.

This report describes performance predictions obtained with a kinetic model of the electrically excited CO laser using either pure CO or CO/N_2/inert diluent. Numerical solutions are obtained for the transient response to an electrical pulse of variable shape and width. The numerical code computes vibrational population distributions, the translational temperature history, spectral distributions of the stimulated flux densities on lasing transitions, and the total output efficiency. Calculations have been made for both multiline lasing operations wherein all transitions reaching the critical threshold gain are assumed to oscillate (non-wavelength selective cavity) and single line/selected multiline calculations corresponding to the use of an intra-cavity wavelength selective element.[10]

The basic kinetics concepts appropriate to the anharmonic molecular laser, characterized by CO, have been presented previously.[3-5] The present report includes a brief description of the kinetic model which incorporates details of the plasma and molecular kinetics including the interactive effects of stimulated emission. The molecular kinetics include both vibration-vibration, V-V, and vibration-translation, V-T, processes among the entire manifold of vibrational levels. The plasma kinetics describe the direct electron impact excitation of the lower vibrational levels. The assumptions and limitations of the model are discussed and reference is given to the kinetic data required in the model.

B. KINETICS

The basic physics describing the kinetic processes appropriate to the electrically excited CO laser are contained in the master vibrational rate equation for the density of molecules in each vibrational level. For pure CO or a mixture of CO and an inert diluent there is just one set of master equations appropriate to each vibrational level of the CO molecule. In the case of mixtures containing another diatomic molecule, such as CO-N_2 mixtures, it is necessary to use a similar set of master equations for each vibrational level of the N_2. For the electrically excited CO laser the master equation can be simply written in the form (for the CO molecules)

$$\frac{dN_v}{dt} = F_{v-1,v} - F_{v,v+1} - D_v + D_{v+1} + E_v + S_{v+1,v} - S_{v,v-1} \qquad (A-1)$$

where

$F_{v,v+1}$ is the net particle flux between levels v and v+1 resulting from V-V collisions

D_{v+1} is the rate of deactivation from level v+1 as a result of V-T collisions and radiative decay

E_v is the net rate of change of N_v as a result of direct electron impact

$S_{v+1,v}$ is the rate of increase in N_v resulting from stimulated emission.

These four terms are described in detail below, together with the assumptions involved in deriving their analytic form.

The V-V and V-T relaxation processes have been considered in detail in previous analysis of vibrational distributions in anharmonic oscillators (e.g., Ref. 3). The assumption is made that only single quantum transitions occur in collisional exchange and one can then write

$$F_{v,v+1} = \sum_M \sum_i \left[k^{v,v+1}_{i,i-1} N_v M_i - k^{v+1,v}_{i-1,i} N_{v+1} M_{i-1} \right] \qquad (A-2)$$

$$D_{v+1} = \sum_M \left[k^{v+1,v}_{V-T} N_{v+1} - k^{v,v+1}_{V-T} N_v \right] M + N_{v+1}/\tau_{v+1} \qquad (A-3)$$

where $k^{v,v+1}_{i,i-1}$ and $k^{v,v+1}_{V-T}$ refer to the rate constants for V-V and V-T exchange respectively, τ_{v+1} is the radiative lifetime of level v + 1 and M is the collision partner. The sources of the relevant rate constants have been described previously.[3] Theoretical calculations as well as recent

experiments[10-13] have shown that the intramolecular V-V processes are extremely rapid in CO. For atmospheric pressure discharges the characteristic V-V time scale is short compared to the time scale for electrical energy deposition in the gas.

The vibrational deactivation by V-T collision is expected to be very slow based on a theoretical extrapolation[3] from the measured deactivation rate constant of the first vibrational level. It is precisely this slow deactivation that permits the relatively efficient operation of the CO laser for long pulse lengths. Unfortunately there is no experimental confirmation of the predicted deactivation rate constants for the high vibrational levels. Furthermore, the practical laser performance may be extremely susceptible to the effect of impurities which can provide large deactivation cross sections.[14-16] There is some experimental confirmation of this effect[17, 18] and it should be pointed out that the very high efficiencies predicted by calculations such as those described in this report may only be achievable in high purity gas systems.

The electron impact excitation function can be written in the form

$$E_v = N_e \sum_i \left(k_e^{i,v} N_i - k_e^{v,i} N_v \right) \qquad \text{(A-4)}$$

where N_e is the electron density and $k_e^{i,v}$ is the rate constant for electron impact excitation from level i to level v. This rate constant requires detailed knowledge of the plasma kinetics. For a uniform discharge with a constant ratio of electric field to gas density, E/N, one solves the Boltzman equation for the non-Maxwellian electron velocity distribution function which is then integrated over the vibrational excitation cross-section data to obtain the necessary excitation rate constants. The accuracy of this approach is dependent upon the accuracy and availability of the necessary excitation cross-section data.[19-21] The electron impact vibrational cross sections have been measured from zeroth to the first nine excited vibrational levels and such cross-section data have been used previously[22, 23] to calculate the electron velocity distribution function. The calculations indicate that the electrical energy is efficiently coupled to the vibrational mode at average electron temperatures of approximately 1 eV with a typical efficiency of over 98%. Recent calculations[24] suggest that the predicted rotational excitation, of the order of 1/2 to 1% of the discharge energy, may be underestimated by an order of magnitude. This would increase the rate of change in the translational temperature which is dominated by V-V vibrational relaxation in the present calculations, the energy defect in the V-V process being taken up in the translation/rotation modes.

Several approximations used in the earlier analyses have been made in the present discharge analysis. Collisions of the second kind were neglected in determining the electron velocity distribution function. Furthermore, electron impact excitation was neglected from any vibrational level other than the zeroth vibrational level. This simply reflects the lack of

theoretical and/or experimental data in CO. Discharge calculations[23] in N_2 have shown that the inclusion of excitation/deexcitation from excited levels leads to a different distribution in the excitation rate constant to the individual vibrational levels. However, the overall excitation rate, $\Sigma v k_v$, was found to be quite insensitive to the excited state distribution. Although these approximations lead to errors in the excitation rate constants they are not expected to have a major effect on the numerical calculations for high pressure electrical lasers. This conclusion follows from considerations of the operating conditions in these lasers, typically electron beam sustained discharges. The pressure is usually high enough so that the characteristic time scale for molecular relaxation processes, of the order of 10^{-6} to 10^{-7} secs, is much smaller than the corresponding time scale for vibrational excitation which is of the order of 10^{-3} to 10^{-5} secs. As a result, errors in the electron impact excitation rate constants to individual vibrational levels tend to get washed out in the vibrational kinetics and the net effect is a small error in the overall excitation rate, $\Sigma v k_v$, which is equivalent to a corresponding change in the electron density and which effect can be estimated from simple scaling considerations described below.

In the determination of the cavity flux it is assumed that the rotational levels are in thermal equilibrium with the translational temperature and that the rotational relaxation is fast enough so that only one rotational line is allowed to oscillate in any given vibrational transition. Furthermore, the cavity flux for each vibrational transition is assumed to be zero unless and until the small signal gain for that particular transition becomes equal to the appropriate cavity loss. After this the steady-state approximation, gain equals loss, is made and the stimulated emission/absorption term is described by

$$S_{v+1,\,v} = g_{v+1,\,v}\,\phi_{v+1,\,v}/h\nu_{v+1,\,v} \tag{A-5}$$

where $g_{v+1,\,v}$ is the saturated gain and $\phi_{v+1,\,v}$ is the cavity flux for the transition $v+1 \rightarrow v$ with frequency $\nu_{v+1,\,v}$. The small signal gain can be shown[25] to be given by an expression of the form

$$g_{\substack{v+1,\,v \\ J-1,\,J}} = K\,\nu_{v+1,\,v}\,J(v+1)\,\Theta_v\,e^{-J(J+1)\,\Theta_v/T} \left\{(1-\epsilon_v)\,N_{v+1}\,e^{2J\left(1+\frac{J-1}{2}\,\epsilon_v\right)\Theta_v/T} - N_v\right\} \tag{A-6}$$

where J refers to the particular rotational level, ϵ_v is a small anharmonic correction to the rotational constant, Θ_v is the characteristic vibrational temperature, and K is a function of the molecular constants together with the line broadening parameters. In the present case, for high pressure electrical discharges the transitions are pressure broadened. An inherent assumption in this analysis is the neglect of spatial variations in the cavity flux. It can be readily shown that the maximum axial variation in the

cavity flux is less than 10% for an output coupling, Lc, of 60% or less. For the present calculations the optical cavity is assumed to be formed by two mirrors of reflectivities R_1 (= 1 - a_1) and R_2 (= 1 - a_2 - Lc) with mirror losses of a_1 and a_2 respectively. Using the steady-state condition $R_1 R_2 \exp(2g\ell) = 1$ it can be shown that the output flux is given by

$$\frac{\phi_{out}}{\phi} = \frac{g\ell\, he}{R_2\left(e^{g\ell} - 1\right)\left(1 + R_1\, e^{g\ell}\right)} \qquad (A-7)$$

where ϕ is the calculated internal cavity flux and ℓ is the length of the active medium.

Before describing the numerical results some comment should be made regarding the expected scaling with gas pressure and electron density. Since only binary collision processes are included in the kinetic model, this scaling is relatively simple. The master equation can be nondimensionalized by the use of particle densities which have been normalized by the total gas density, N. The collisional terms can then be written directly in terms of these normalized densities and the term containing the natural lifetime can be neglected in comparison with the V-V and stimulated emission terms. The electron density becomes normalized by the total gas density and the dimensionless stimulated emission term behaves like ϕ/N^2 as a result of the small signal gain varying with total gas density and inversely with the pressure broadened linewidth. It follows then that for fixed ratio of electron density to total gas density, Ne/N, the flux should scale with the square of the gas density, $\phi \sim N^2$, and the time should scale inversely with gas density, $\tau \sim N^{-1}$. In this simple scaling relation the effect of temperature variations on the collisional rate constants and the line broadening have been neglected. The errors introduced by this approximation have been shown to be negligible by numerical calculations.

C. NUMERICAL RESULTS AND DISCUSSION

Some standard operating conditions which are characteristic of high pressure discharge lasers have been chosen for the present numerical calculations of the transient response to a pulsed discharge. Furthermore, the present calculations have been restricted to the case of pure CO or mixtures of CO - N_2. Although CO-Ar mixtures are of interest in practical systems, the expected performance with such mixtures can be readily derived from considerations of pure CO at the same value of E/N where the N refers to the CO density alone. The reasons for this are as follows:

1) The Ar is virtually transparent to the low energy electrons (of the order of 1 eV) because of the characteristic Ramsauer dip[26] and the fact that the lowest electronic state is over 11 eV above the ground state.

2) The Ar plays virtually no role in the kinetic relaxation processes because it only interacts in the V-T deactivation process and this is always negligible compared with the V-V intramolecular exchange process.

The major difference between the results predicted for pure CO and that for CO-Ar mixtures at the equivalent E/N, is due to the change in heat capacity which modifies the translational temperature rise. The pressure broadening of CO by Ar is similar in magnitude to the self-broadening[27] so that the addition of Ar will not affect the small signal gain at the same total pressure. These comments assume the same ratio for electron density to total CO density.

Since most practical high power electrical lasers such as the electron beam sustained discharges[7, 28] operate at or near atmospheric pressure, the present calculations have been made at a fixed total gas density of one amagat corresponding to a pressure of approximately one atmosphere at room temperature. The temperature range of interest from $50^{\circ}K$ to $300^{\circ}K$ was chosen as being representative of the temperature range of operation from approximately liquid N_2 temperature to room temperature. In principle one would like to operate the discharge at E/N of approximately 5×10^{-16} volt-cm^2 to obtain an electron temperature of the order of one eV and so optimize the rate of the energy transfer into the vibrational mode by electron impact.[22, 23] In practice for pulse lengths of the order of 10 μsec or longer, the maximum E/N is limited by arcing due to inevitable field concentrations. A practical operating value of E/N of the order of 2×10^{-16} volt-cm^2 was chosen for these calculations as being representative of experimentally achievable discharge conditions. This corresponds to an electron temperature of approximately .7 eV in pure CO and .9 eV in a mixture of 10% CO - 90%N. At room temperature this is equivalent to an applied electric field of 5,000 volts per atm-cm and corresponds to an overall excitation rate constant, $\Sigma v k_v$, of approximately 2.5×10^{-9} cm^3 per second.

An electron density of 10^{13} per cubic centimeter was chosen for these calculations being representative of the electron density readily achievable with a practical electron beam gun[28] operating at a current density of the order of 10 mamp per square cm. For a discharge dominated by dissociative recombination losses, as typified by CO-N_2 discharges, the electron density varies with the square root of the electron beam current density. The present calculations assume a constant electron density and neglect the small but finite rise time due to electron loss processes following the discharge initiation. This can be readily included in calculations for detailed comparison with experiment but has a small effect on the lasing pulse shape and does not influence the parametric dependencies discussed in this report.

Using the above discharge conditions, several calculations were made to determine the effect of output coupling on the total electrical efficiency for representative CO-N_2 mixtures. These calculations covered a range of output coupling from 10 to 90% for the assumed 1 meter discharge length and indicated comparable operating efficiency at output couplings above 25%. The efficiency decrease observed with low output couplings results from the rapid increase in the gas translational temperature as a result of the inefficient coupling. It was decided to do all

the subsequent calculations using a representative value of 30% for the output coupling and an assumed 3% reflectivity loss due to absorption at each mirror.

The sensitivity of both the total electrical efficiency and the energy distribution to the initial translational temperature is shown in Figs. 2 and 3. These calculations have all been made for a 20% mixture of CO in N_2 with a total gas density of 1 amagat. Figure 2 shows the variation in the total efficiency for both multiline output, i.e., where all transitions which reach the threshold conditions are allowed to oscillate, and for two single-line conditions in which the output was restricted to a single vibration/rotation transition from vibrational levels $10 \rightarrow 9$ and $5 \rightarrow 4$. The total electrical efficiency is here defined as the ratio of the energy coupled out of the cavity to the total electrical input into the discharge and, therefore, does not include losses into the mirrors which have been assumed to be 15% relative to the output flux as discussed above. Since the efficiency is time dependent what has been plotted in Fig. 2 is the maximum value of the total integrated electrical efficiency. The local or instantaneous efficiency is initially zero and once threshold gain conditions have been reached, rises rapidly to an almost constant value and after some time starts to decrease as a result of the increasing translational temperature. As a result the total integrated electrical efficiency rises somewhat more slowly to a maximum value which has been plotted in Fig. 2, the typical times to reach maximum efficiency being of the order of 30 to 100 microseconds for the assumed discharge conditions. These times could be scaled to other discharge conditions by the simple scaling relationships discussed earlier.

The temperature dependence of the multiline efficiency is to be expected based on considerations of small signal gain and vibrational relaxation. The gain in a partial inversion as described in Eq. (A-6) is clearly a very sensitive function of the translational temperature and for a given vibrational distribution, increases rapidly with decrease in translational temperature. Thus, the time to reach threshold gain increases with the translational temperature and as a result the amount of energy which must be invested in the vibrational mode in order to reach threshold conditions also increases drastically with translational temperature. These effects are clearly seen in Fig. 3 in which is shown the fraction of the total input electrical energy stored in vibrational and rotational/translational energy as a function of time for each of the three different temperatures corresponding to the multiline calculations in Fig. 2. The variation in the time necessary to reach threshold conditions, indicated by the rapid drop in the fraction of energy stored in vibration, is evident in Fig. 3 and is a minimum at the lowest translational temperature. Similarly the fraction of energy stored in vibration is a minimum at the lowest temperature. This figure also illustrates the approach to the quasi-steady-state conditions following which the stored vibrational energy must continue to increase slowly to maintain the cavity gain requirement as the translational temperature increases.

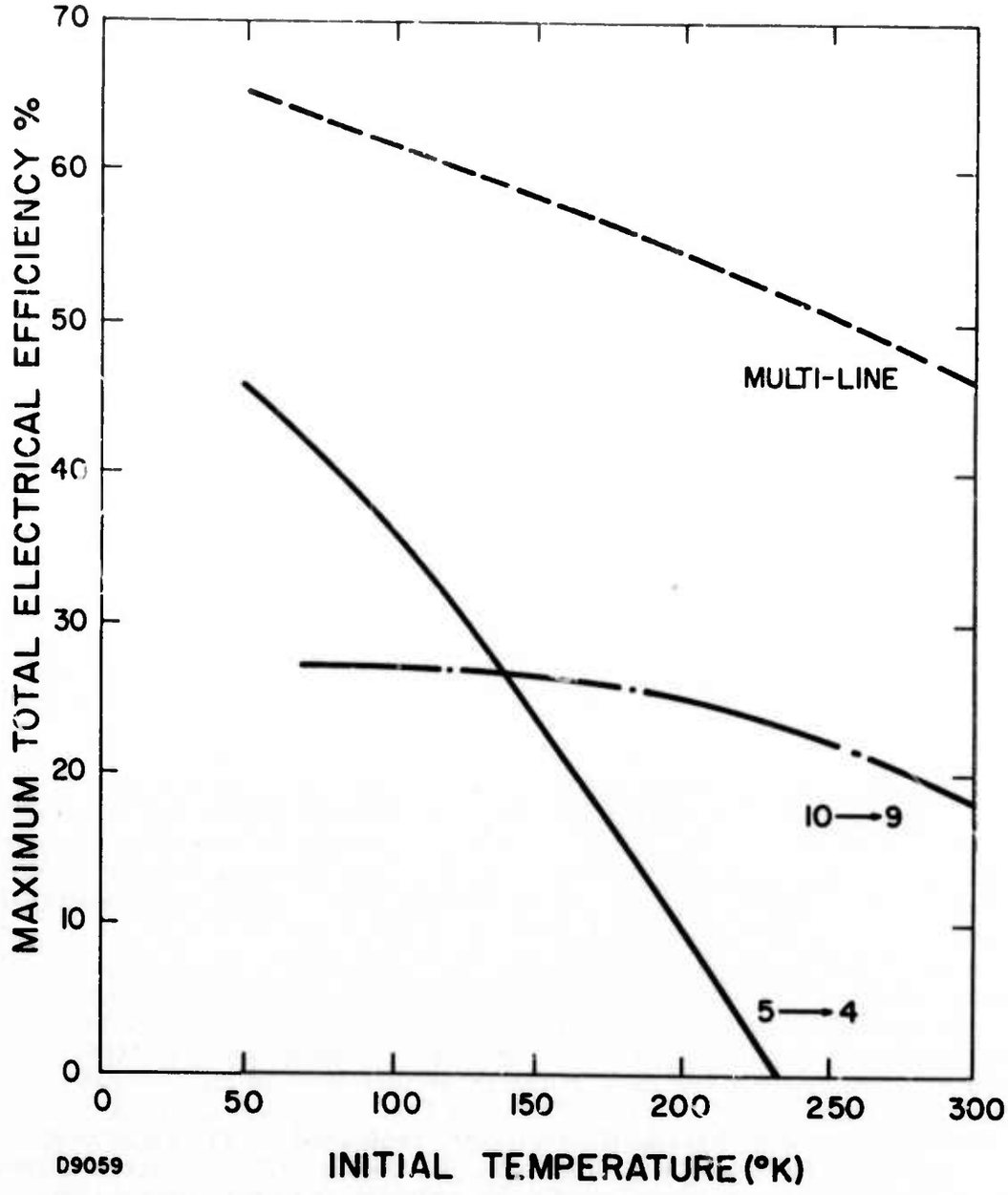

Fig. 2 Sensitivity of the Maximum Total Electrical Efficiency to the Initial Translational Temperature under Single and Multiline Conditions. $N_e = 10^{13}$ cm^{-3}, $\psi CO = 0.2$, $E/N = 2 \times 10^{-16}$ volt-cm^2 and $N = 2.69 \times 10^{19}$ cm^{-3}. The active discharge length is 100 cm and the output coupling is 30% with an additional 6% loss in mirror reflectivity.

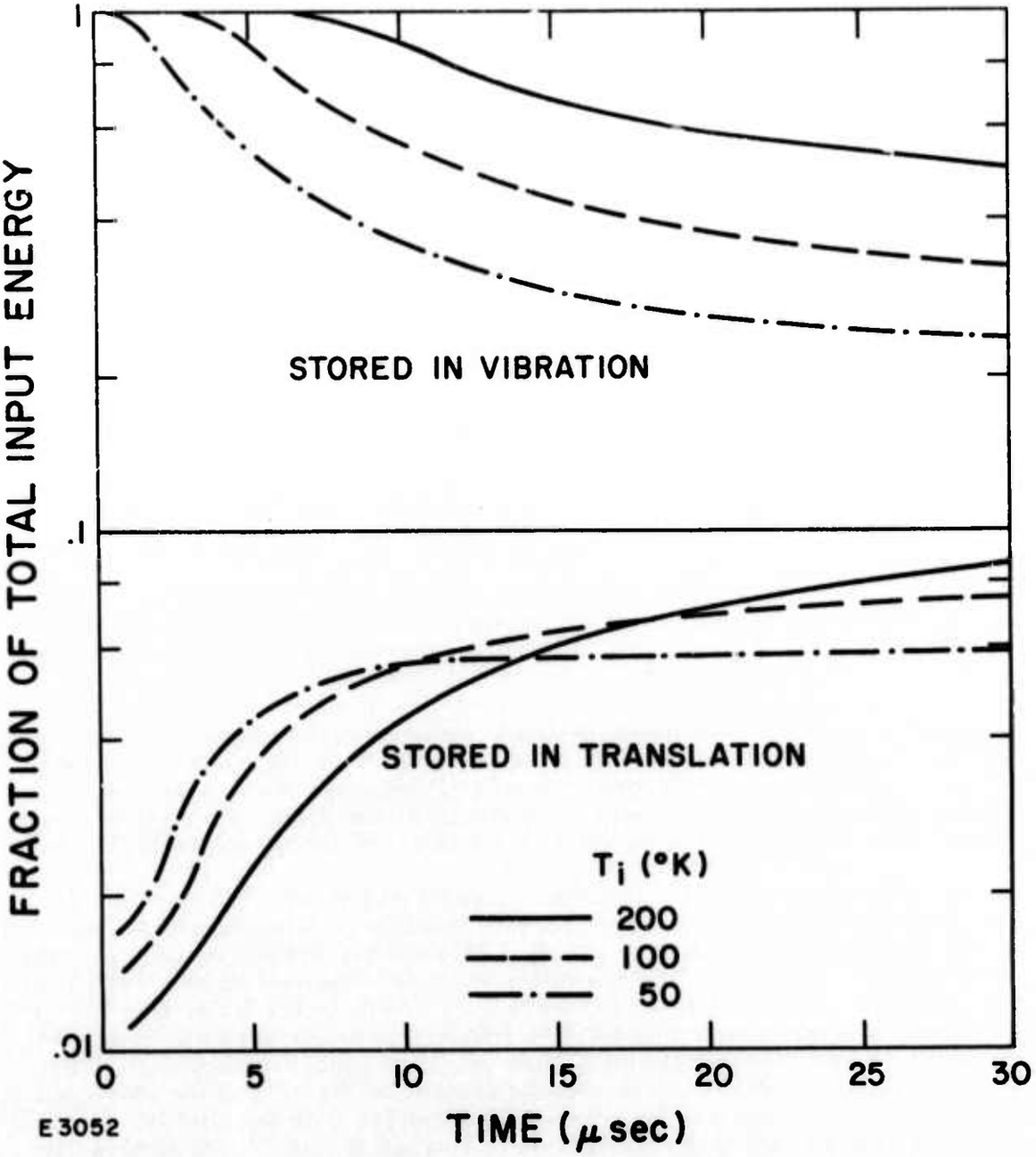

Fig. 3 Energy Storage in the Vibrational Mode and the Translational/ Rotational Modes under the Same Multiline Conditions as in Fig. 2.

The net rate of the V-V relaxation in the CO increases with decreasing translational temperature primarily as a result of detailed balancing. (The forward or exothermic rate constants for near resonant collisions, which dominate the relaxation process, have been shown theoretically[3] and experimentally[10-13] to be quite insensitive to the translational temperature.) Since the translational temperature is controlled by the V-V relaxation, the initial energy flow to translation/rotation increases with decreasing translational temperatures as shown in Fig. 3. However, the rate dT/dt decreases with time as one approaches the quasi-steady state and the calculations for the highest initial translational temperature ultimately yield the highest fraction of energy in translation. The lower translational temperatures favor lasing on lower vibrational levels than for conditions at high translational temperatures as described in detail below. As a result, energy has to be transferred further up the vibrational ladder under high translational temperature conditions with consequent increased heating of the gas due to the V-V relaxation.

The cavity flux on each oscillating transition is shown in Fig. 4 over the range of temperatures used for the multiline calculation in Figs. 2 and 3. A peak in the cavity flux distribution is always seen to occur near the lowest oscillating transition and the flux distributions fall off steeply at higher vibrational levels. This results from the fact that electron energy is pumped predominantly into the lower vibrational levels and V-V relaxation then redistributes this energy to the higher vibrational levels. The lowest vibrational level for which the threshold gain condition is reached is dependent upon the translational temperature because of the sensitivity of the small signal gain to this temperature as described in Eq. (A-6). The distributions shown in Fig. 4 have been plotted for the pulse times corresponding to the maximum value of total efficiency shown in Fig. 2. The decreasing slope of the flux distributions at the higher translational temperatures results from the necessity to increase the energy stored in vibration in order to maintain the cavity gain condition. This effect, in turn, leads to an increase in the V-V transfer of energy to the higher level.

Also shown in Fig. 2 is the variation of the total efficiency with translational temperature under single transition operating conditions such as would be obtained with the use of an intracavity grating or prism. The efficiency on any single-line operation must be expected to be smaller than the corresponding multiline efficiency as a result of the finite rate for vibrational relaxation and the fact that this relaxation occurs via both near neighbor (nearly resonant) and distant neighbor (nonresonant) collisions. This decrease in efficiency is clearly evident in Fig. 2 and the steep falloff in total efficiency for the $v=5 \rightarrow v=4$ transition with translational temperature is expected from the flux distributions in Fig. 4. It is directly attributable to the variation of gain with T. The efficiency for single-line lasing on higher level transitions as shown for $10 \rightarrow 9$ is far less sensitive to the translational temperature since this transition is beyond the peak of the flux distributions for all but the highest translational temperature and hence the vibrational energy is cycled through this level.

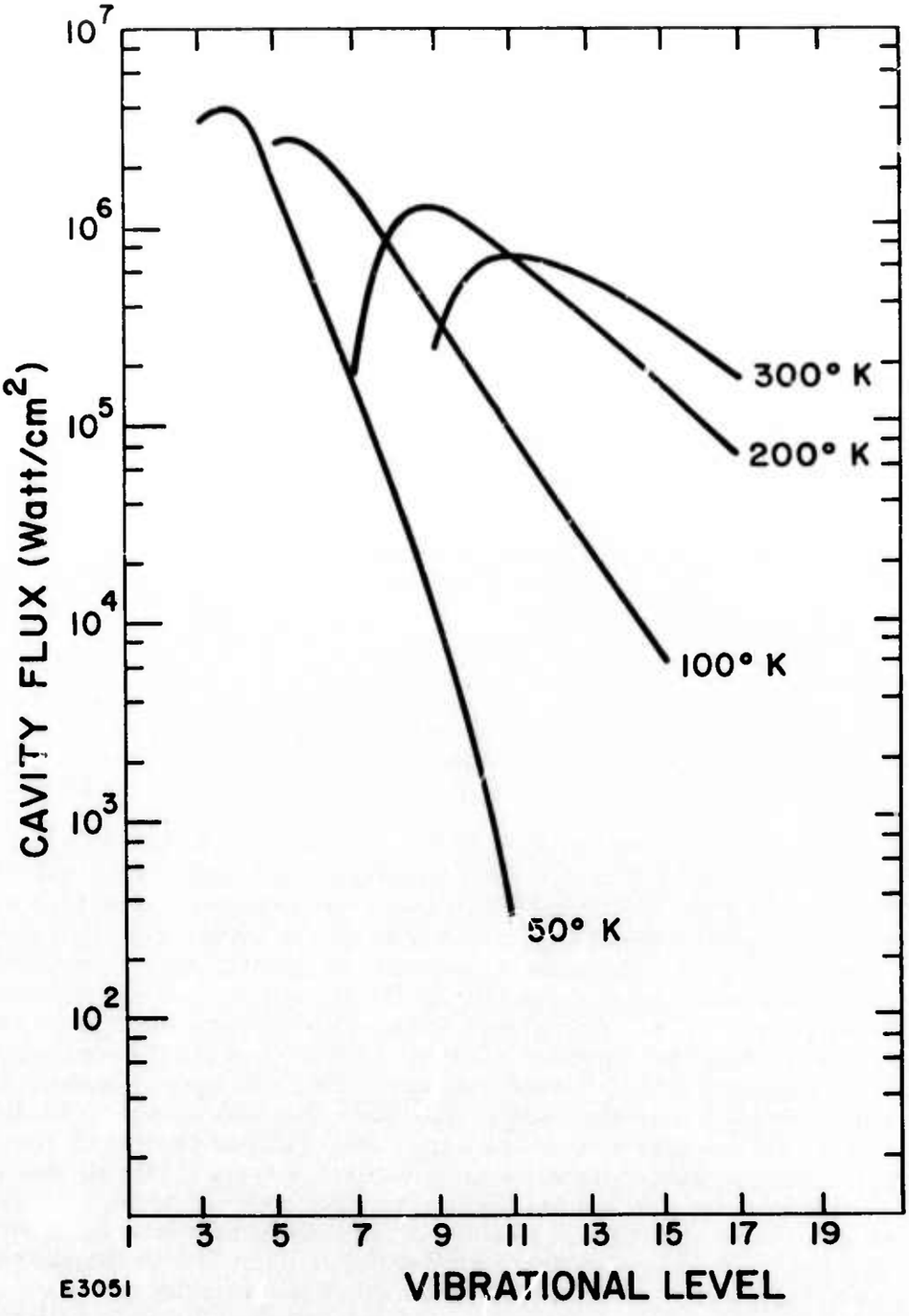

Fig. 4 Cavity Flux Distribution at the Maximum Total Efficiency for the Same Multiline Conditions Shown in Fig. 2.

The flux extracted in a single vibrational transition is always as large or larger than the energy extracted in the same transition under multiline operating conditions. Clearly for vibrational levels below the level of the peak in the distribution $\phi^{v, v-1}_{single}$ is approximately equal to $\phi^{v, v-1}_{multi}$ because the same amount of energy flows through the level v under each operating condition. On the other hand for vibrational levels beyond the peak in the multiline distribution $\phi^{v, v-1}_{single}$ is greater than $\phi^{v, v-1}_{multi}$ since the vibrational relaxation process transfers energy preferentially up the ladder. As a result the vibrational energy cannot escape via the lower level transitions which would oscillate under multiline conditions and therefore is cycled through the higher level transitions.

As indicated earlier the total electrical efficiency passes through a maximum in time because of the temporal increase in the translational temperature. The rate of increase dT/dt is clearly greater for single-line than multiline operation because it results from the anharmonic energy defect which is converted to translational/rotational energy in the V-V relaxation process. For single-line operation, the vibrational quanta have cycled through more vibrational levels than in the multiline process until the quanta reach a vibrational level where they can escape via stimulated emission or be quenched by V-T collisions at even higher levels. For the assumed operating conditions the rate of increase of the translational temperature can be 50% larger for the single-line operation relative to the multiline. For single-line operation from v to v-1 the gradient dT/dt increases with the increasing level v beyond the peak of the flux distribution.

All calculations shown until now have been made to illustrate the effect of varying the initial translational temperature. It is also of interest to predict the performance variation with gas mixture and such calculations are shown in Fig. 5. Here the maximum total efficiency is plotted as a function of the mole fraction of CO in CO-N_2 mixtures for a constant initial temperature of 100°K. As before, these calculations have been made for a fixed electric field or constant value of E/N. To a first order approximation, the overall excitation rate constant, $\Sigma v k_v$, is approximately independent of the CO mole fraction ψ_{CO}. Because the vibrational excitation cross sections of CO peak at a lower electron energy than the cross sections for N_2 the discharge tends preferentially to excite the CO vibrational levels. As a result the net vibrational excitation rate per CO molecule increases almost inversely with the CO mole fraction down to mixtures of 20% CO. Even for mole fractions as low as $\psi_{CO} = 0.1$ only 20% of the energy is coupled directly to the N_2 and 80% into the CO. In principle the N_2 vibrational energy should be transferred via intermolecular V-V collisions to the CO molecule since this exchange is exothermic. However, the cross section for this exchange process[12, 29, 30] is three orders of magnitude smaller than the cross section for intramolecular transfer in the CO molecule. This transfer from N_2 to CO is therefore too slow to be effective for pulse lengths of the order of 100 μsecs or less. On the other hand

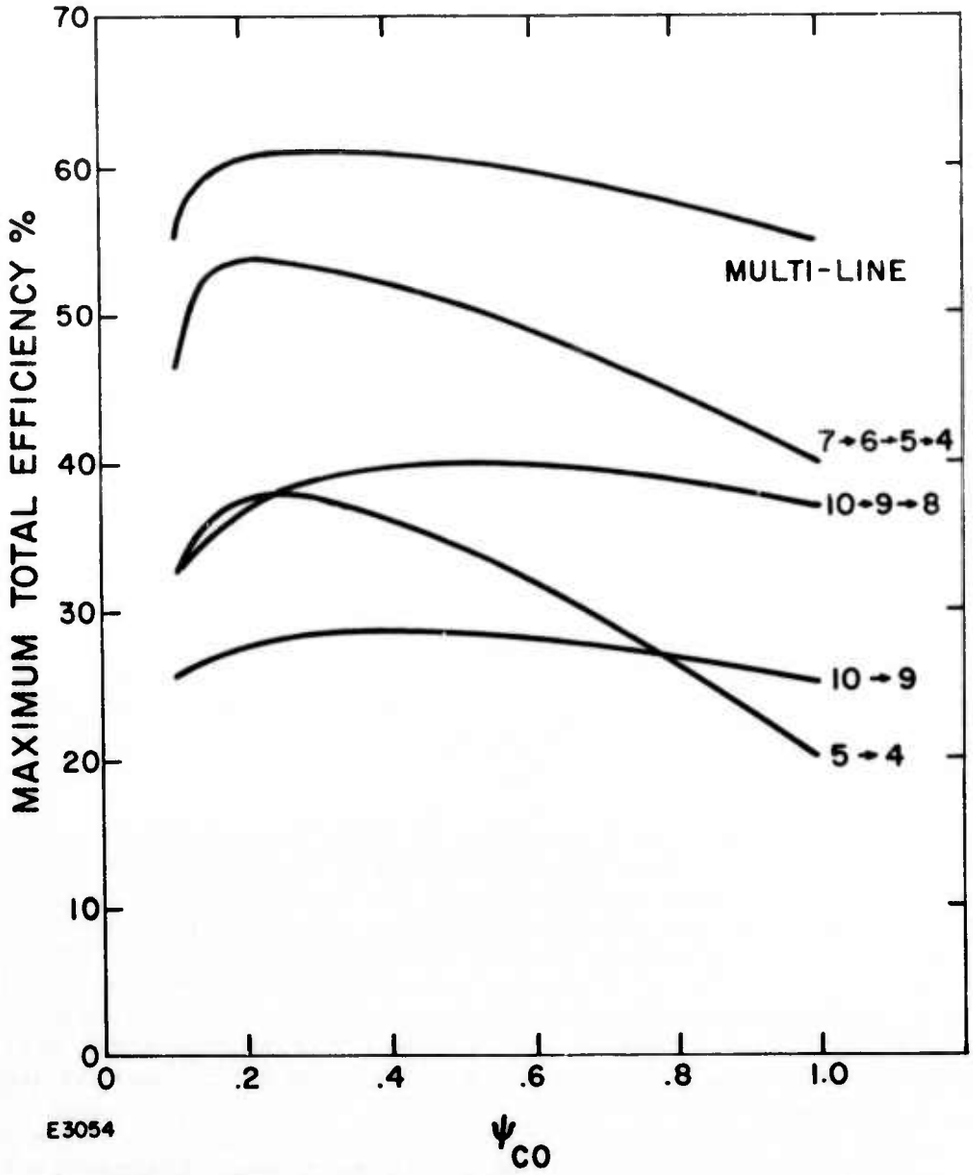

Fig. 5 Variation of Maximum Total Efficiency with the CO Mole Fraction under Selected Line and Multiline Operation. The discharge and cavity conditions are the same as in Fig. 2.

this intermolecular transfer is clearly important in cw CO lasers and is probably responsible for the recent research experimental observation[31] of lasing on the lowest transition v=1 → 0, in a low pressure discharge tube experiment using very dilute mixtures of CO in N_2 and He.

The results shown in Fig. 5 indicate that the multiline efficiency should be relatively insensitive to the CO mole fraction, peaking with a maximum efficiency occurring at mole fractions of the order of 20 to 30% as has been observed experimentally.[28] The efficiency decrease with decreasing mole fraction below $\psi_{CO} = 0.2$ is due to the electron excitation of vibrational mode of N_2 and lack of V-V transfer from N_2 to CO. It should be noted here that the predicted delay time to reach the threshold conditions (the time from the discharge onset to the lasing onset) decreases with decreasing CO mole fraction as has been observed experimentally.[28] This change in the threshold delay time results from the increase in the vibrational energy per CO molecule, and consequent increase in the effective local vibrational temperature, as the mole fraction decreases. Thus, at any time before lasing the small signal gain is expected to increase inversely with the CO mole fraction (see Eq. (A-6)). This gain variation also implies that the lowest lasing transition moves to lower vibrational levels as ψ_{CO} is decreased. Correspondingly, the vibrational distribution flattens out as ψ_{CO} increases because of the increased rate of vibrational relaxation with increasing mole fraction. These effects are responsible for the sensitivity of the low-level single-line performance with CO mole fraction as illustrated in Fig. 5, i.e., the sensitivity of the low level, v=5 - 4, single-line performance to ψ_{CO} is the direct result of the influence of the CO mole fraction on the vibrational energy per molecule and hence the small signal gain.

Also shown in Fig. 4 are some calculations for several selected lines to simulate conditions one might achieve by use of an intercavity water vapor absorption cell.[32] The efficiency for operation from v=7 → 6 → 5 → 4 is close to the multiline efficiency for small mole fractions since these transitions are near the peak in the multiline flux distribution (compare with Fig. 4). For lasing on the transition v=10 → 9 or v=10 → 9 → 8 the total efficiencies are much greater than for the corresponding transitions under multiline operation (by over an order of magnitude) because of the preferential transfer of vibrational energy up the vibrational ladder as discussed earlier.

The effect of varying the electron density while keeping the total gas density and the gas mixture constant is shown in Fig. 6. The solid curves correspond to an initial translational temperature of 100°K and the dashed curve and initial translational temperature 300°K assuming multiline operation in a 20% mixture of CO in N_2. In this figure the time scale $N_e t$ has been used since the rate of vibrational excitation by electron impact varies directly with the electron density. This electron excitation is the rate limiting process since the characteristic time for V-V exchange is much smaller than the characteristic time for electron excitation of vibration under the present assumed conditions.

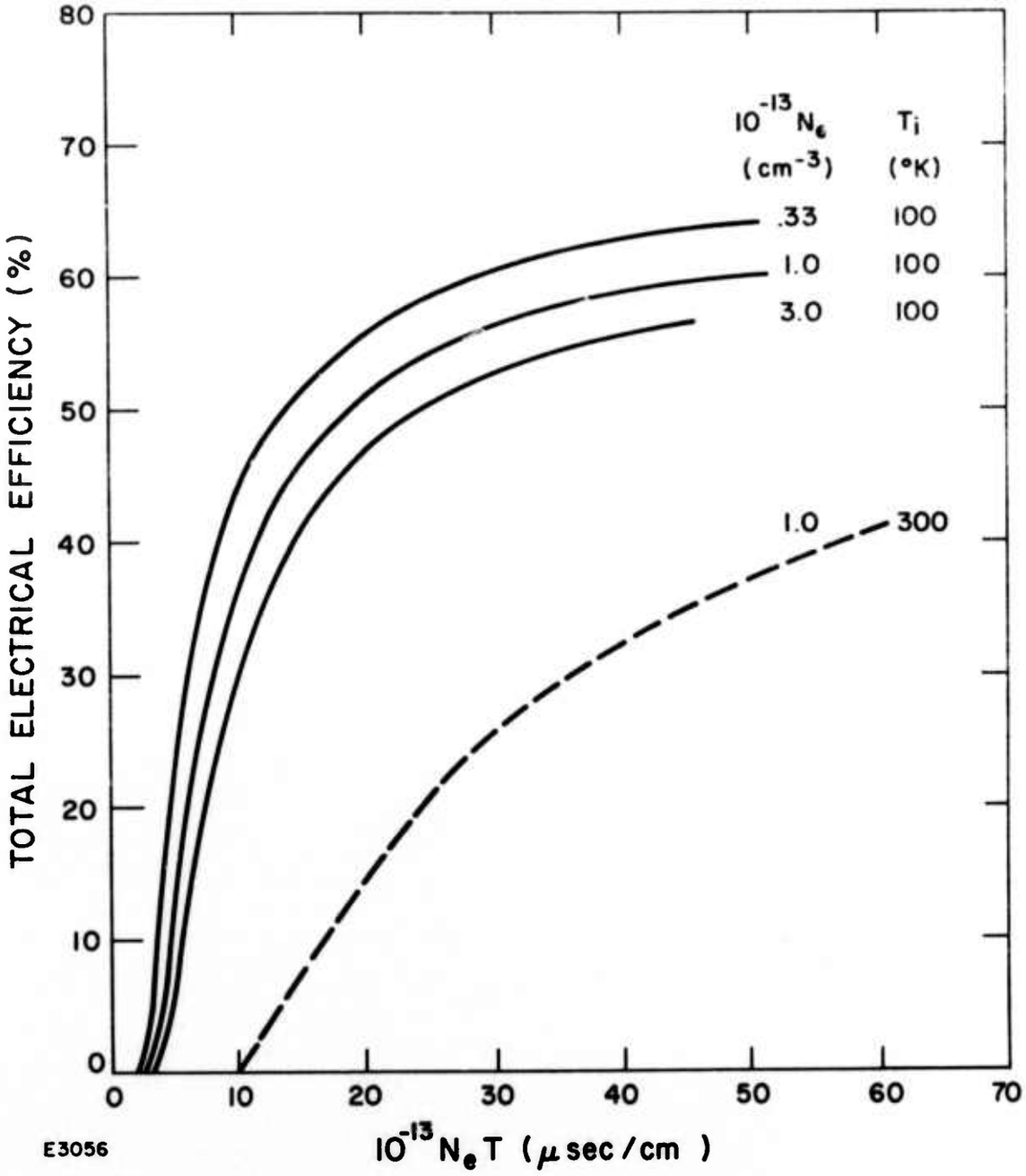

Fig. 6 Temporal Variation of the Total Multiline Efficiency for $\psi_{CO} = 0.2$ and Several Values of N_e and the Initial Translational Temperature, Ti. All other conditions are the same as in Fig. 2.

The calculations indicate that the delay time to reach the threshold conditions varies as Ne^{-a} where $a < 1$ whereas one would expect $a = 1$ in the absence of vibrational relaxation. The departure from the expected N_e^{-1} behavior in the time scale is small compared with the overall variation in N_e, an order of magnitude in the present calculations. Although not shown in this figure the calculations also indicate that the vibrational level for the lowest transition decreases with increasing electron density. This occurs because of the finite rate of the V-V relaxation with the result that the effective vibrational temperature (and correspondingly the small signal gain) in the lower levels increases with increasing N_e at fixed value of $N_e t$. The small shift in the lasing transitions towards lower vibrational levels with increasing N_e also results in a small decrease in the total efficiency because a greater fraction of the total energy must be stored in the vibrational distribution to maintain the lower level inversion.

The temporal variation in the translational temperature is shown in Fig. 7 for the same conditions as used in Fig. 6 time being again normalized by the electron density. In all these calculations, the dominant gas heating term results from the anharmonic V-V exchange collisions for which the energy defect is absorbed in translation. The gas heating can be approximately represented by

$$N C_p \frac{dT}{dt} \sim k_{v-v} N^{\dagger 2} \qquad \text{(A-8)}$$

where $N^\dagger$ represents the population density of the vibrationally excited CO. By reference to the master equation (A-1), one can deduce that $k_{v-v}N^{\dagger 2} \sim k_e N_e N$ so that $dT/dt \sim k_e N_e / C_p$ and one would expect the temperature increase to scale as $N_e t$. This is verified to first order by the calculations shown in Fig. 7. The perturbation from the predicted result indicates a small relative increase in ΔT with decreasing N_e. This arises from the small shift in the lasing flux distribution to higher vibration levels as N_e decreases thereby requiring vibrational quanta to be transferred further up the vibrational ladder before they can escape via stimulated emission. The fractional temperature rise with a 300°K initial condition is significantly smaller than the corresponding temperature rise at the 100°K initial condition and is simply related to the much longer characteristic time scales for the high temperature operating conditions.

Finally, some calculations were made to examine the effect of maintaining fixed power input, i.e., $N_e N$ constant while allowing both the electron density N_e and the total gas density N to vary. These calculations were made for 20% mole fraction of CO in N_2 and are shown in Fig. 8. The data are plotted against the normalized time scale $N_e t$ since this characterizes the fractional excited population of the CO. Because the small signal gain is a function of the total CO density as well as vibrational energy per CO molecule, it follows that the time to reach threshold conditions must decrease with increasing CO density as illustrated in Fig. 8. Unfortunately, there does not appear to be any simple interpretation for the variation in total efficiency calculations under these constant input power conditions. The variation in the translational temperature for these constant input power conditions are similar to the results shown in Fig. 7 and to first order exhibit the same expected temperature scaling, namely ΔT varying as $N_e t$.

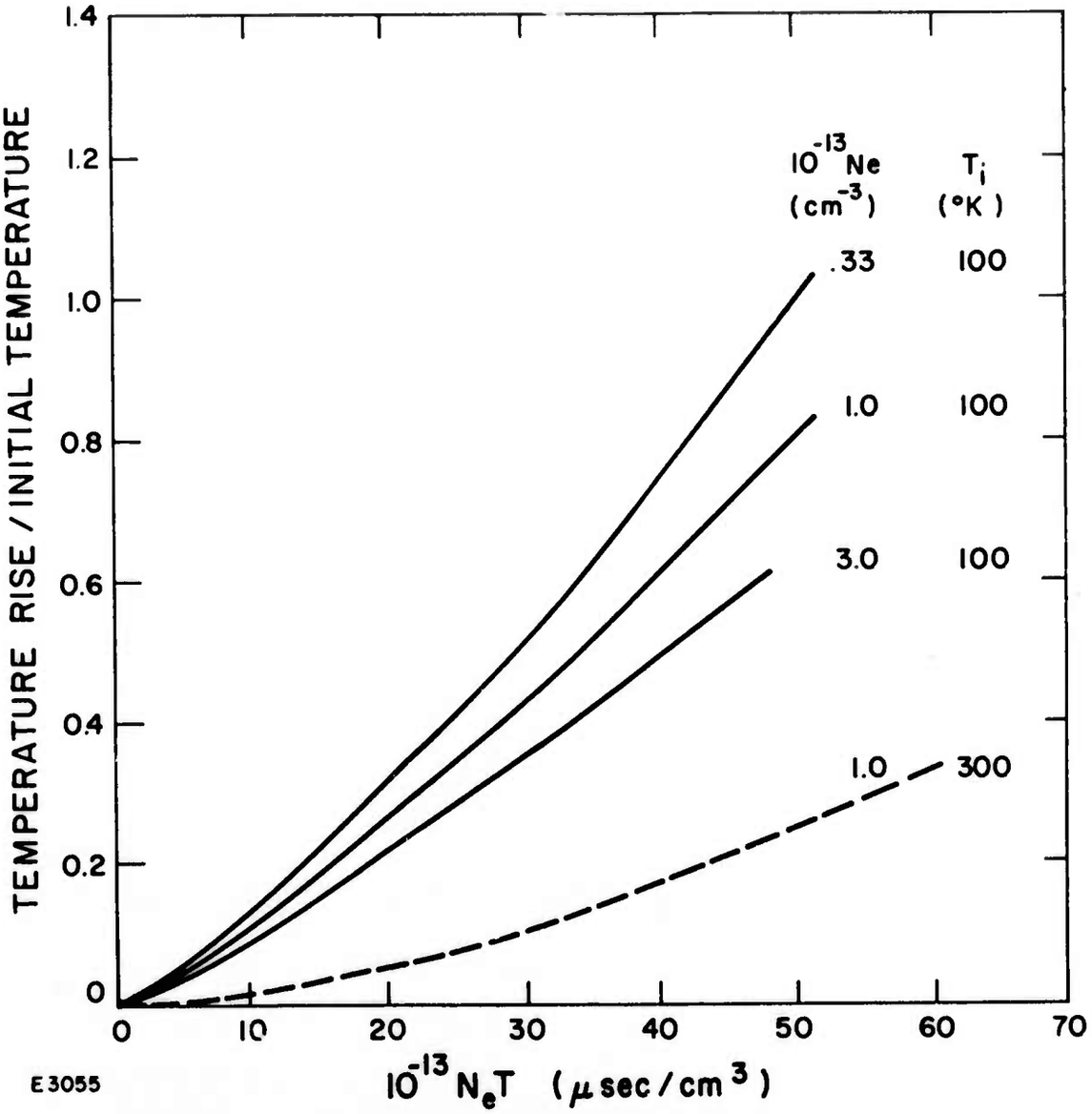

Fig. 7 Temporal Variation in the Translation/Rotation Temperature Corresponding to the Efficiency Calculations in Fig. 6.

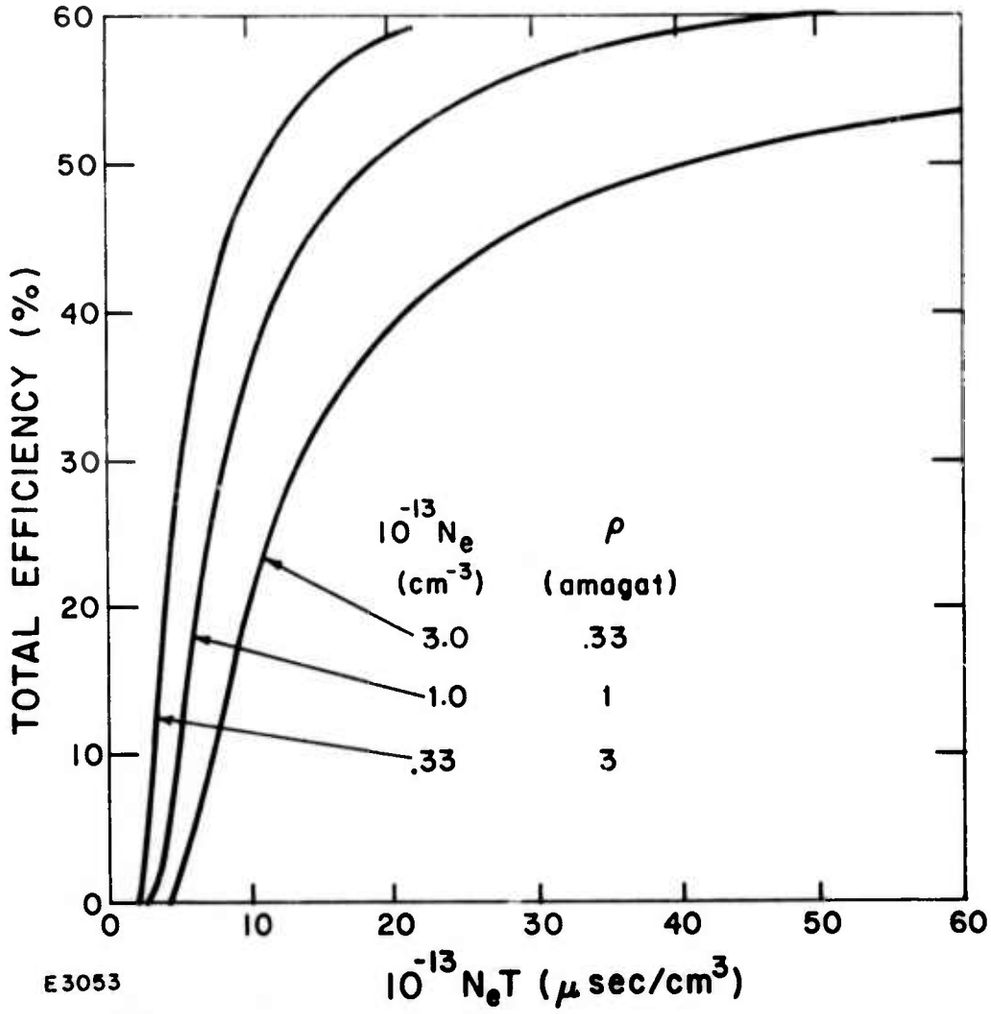

Fig. 8 Variation in Total Multiline Efficiency with Time for Constant Power Input, N_e N = Constant, at an Initial Translational Temperature of 100°K. All other conditions are the same as in Fig. 2.

APPENDIX A

REFERENCES

1. Bhaumik, M. H., Lacina, W. B. and Mann, M. M., IEEE J. Quantum Electron, QE-8, 150 (1972).

2. Mann, M. M., Rice, D. K. and Eguchi, R. G., to be presented at VIII Int. Quantum Electron. Conf., San Francisco (1974).

3. Caledonia, G. E. and Center, R. E., J. Chem. Phys. 55, 552 (1971).

4. Center, R. E. and Caledonia, G. E., Appl. Phys. Letters 19, 211 (1971).

5. Rich, J. W., J. Appl. Phys. 42, 2719 (1971).

6. Jeffers, W. Q. and Wiswall, C. E., J. Appl. Phys. 42, 5059 (1971).

7. Lacina, W. B., Mann, M. M. and McAllister, G. L., IEEE J. Quantum Electron. QE-9, 588 (1973).

8. Abraham, G. and Fisher, E. R., J. Appl. Phys. 43, 4621 (1972).

9. Rockwood, S. D., Brau, J. E., Proctor, W. A. and Canavan, G. H., IEEE J. Quantum Electron. QE-9, 120 (1973).

10. Smith, I. W. M. and Wittig, C., Faraday Transactions II, 7, 939 (1973).

11. Sackett, P. B., Hordvik, A. and Schlossberg, H., Appl. Phys. Lett. 22, 367 (1973).

12. Stephenson, J. C., Appl. Phys. Lett. 22, 576 (1973).

13. Powell, H. T., J. Chem. Phys. 59, 4937 (1973).

14. von Rosenberg, C. W., Jr., Taylor, R. L. and Teare, J. D., J. Chem. Phys. 54, 1974 (1971).

15. von Rosenberg, C. W., Jr. and Wray, K. L., J. Chem. Phys. 54, 1406 (1971).

16. Center, R. E., J. Chem. Phys. 58, 5230 (1973).

17. Boness, M. J. W. and Center, R. E., Section II of this report.

18. Mann, M. M., private communication.

19. Schulz, G. J., Rev. Mod. Phys. 45, 423 (1973).

20. Ehrhardt, H., Langhans, L., Linder, F. and Taylor, H. S., Phys. Rev. 173, 222 (1968).

21. Boness, M. J. W. and Schulz, G. J., Phys. Rev. A 8, 2883 (1973).

22. Hake, R. D., Jr. and Phelps, A. V., Phys. Rev. 158, 70 (1967).

23. Nighan, W. L., Appl. Phys. Lett. 20, 96 (1972).

24. Chandra, N. and Burke, P. G., J. Phys B: Atom. Molec. Phys., 6, 2355 (1973).

25. Penner, S. S., Quantitative Molecular Spectroscopy and Gas Emissivities, Addison-Wesley, Reading, Mass. (1959).

26. Massey, H. S. W. and Burhop, E. H. S., Electronic and Ionic Impact Phenomena, Vol. I, Oxford, Clarendon Press (1969).

27. Robinson, C. Crane and Thompson, H. W., Proc. Roy. Soc. 272A, 441 (1963).

28. Center, R. E., IEEE J. Quantum Electron. QE-10, 208 (1973).

29. Zittel, P. F. and Moore, C. B., Appl. Phys. Lett. 21, 81 (1972).

30. Green, W. H. and Hancock, J. K., IEEE J. Quantum Electron. QE-9, 50 (1973).

31. Djeu, N., Appl. Phys. Lett. 23, 309 (1973).

32. Bhaumik, M. L., Appl. Phys. Lett. 20, 342 (1972).

APPENDIX B

LINESHIFT/LINEWIDTH CALCULATIONS

A. INTRODUCTION

Most theories of pressure shift (and broadening) are based on Anderson's theory,[1] and our analysis will follow the general outlines set down by Anderson. We shall be interested in radiating molecules perturbed by intermolecular collisions, specifically CO perturbed by N_2. Measurements of CO shift induced by the noble gases in collisions have been reported[2] and are of the order of 5 cm^{-1}/atm. However, CO-N_2 shifts have not yet been measured, and a theoretical analysis was necessary.

The problem of line shifts by intermolecular collisions was previously investigated by Sharma and Caledonia,[3] who applied their results to the vibrational-rotational spectra of DCl perturbed by HCl and HCl perturbed by DCl. We have applied our analysis to these cases as well, checking our calculations against the experimental results of Jaffe[4] and his co-workers. We obtain somewhat better agreement than that obtained in Ref. 3. Finally, the CO-N_2 shifts have been found to be of the same order as the measured CO-rare gas shifts.

In the discussion below we present an outline of the problem and the highlights of the analysis, as well as compendium of the obtained results.

B. STATEMENT OF THE PROBLEM

The physical origin of the line shift lies in the fact that the molecular interaction energy is, in general, not the same in the upper and lower states of the radiative transition.

Consider a radiating molecule being perturbed by another molecule passing close by. The amplitude of the radiation is proportional to the autocorrelation function. Thus, if $|i\rangle$, $|f\rangle$, denote initial and final states,

$$\text{Amplitude} \sim \langle f | \mu(t) | i \rangle \tag{B-1}$$

where μ is the dipole moment, and

$$\text{Intensity} \sim \langle \mu(t) \mu(t+\tau) \rangle \tag{B-2}$$

Now, if H_c denotes the interaction

$$(m|\mu(t)|n) \approx \mu_{mn}(0)\exp\frac{1}{i\hbar}\left[(E_m - E_n)t + \int_o^t \left[(m|H_c|m) - (n|H_c|n)\right] dt'\right] \quad (B-3)$$

If we write the spectral density as the transform of an autocorrelation function, we have

$$I(\omega) \sim \int d\tau \left[\exp i(\omega_{mn} - \omega)\tau\right] \Phi(\tau) \quad (B-4)$$

where $\Phi(\tau)$ is that part of the autocorrelation function not included in the sinusoidal variation, and may be written as

$$\Phi(\tau) = \int dt \exp\left[i(\eta_{if}(t+\tau) - \eta_{if}(t))\right] \quad (B-5)$$

where

$$\eta_{if}(t) \equiv \frac{1}{i\hbar}\int_o^t \left[(m|H_c|n)\right] dt' . \quad (B-6)$$

Now

$$\eta_{if}(t+\tau) - \eta_{if}(t) = \sum_{\substack{\text{collisions from} \\ t \text{ to } t+\tau}} \eta_c \quad (B-7)$$

and $\Phi(\tau)$ has the form

$$\Phi(\tau) \sim \langle \exp i \left[\sum \eta_c\right] \rangle . \quad (B-8)$$

By the central limit theorem $\sum \eta_c$ will be a Gaussian random variable. For such a variable

$$\Phi(\tau) \sim \exp i \langle \sum \eta_c \rangle \exp -\frac{1}{2} \langle \left(\sum \eta_c\right)^2 \rangle . \quad (B-9)$$

Now

$$< \sum \eta_c > = < \eta > \times \frac{\text{collisions}}{\text{unit time}} \times \tau \approx < \eta > n\sigma v\tau \qquad \text{(B-10)}$$

where v is the relative velocity, n the perturber density per unit volume, and σ is the collision cross section. Similarly

$$< \left(\sum \eta_c \right)^2 > = < \eta^2 > n\sigma v\tau . \qquad \text{(B-11)}$$

Hence

$$I(\omega) \sim \frac{1}{(\omega - \omega_{ij} - nv\sigma_i)^2 + (nv\sigma_r)^2} \qquad \text{(B-12)}$$

where (X denotes a sample over collision events),

$$\sigma_r = \frac{\sigma}{2} \int dX \, \eta^2 \equiv \frac{\sigma}{2} < \eta^2 > \qquad \text{(B-13)}$$

and

$$\sigma_i = -\sigma \int dX \, \eta = -\sigma < \eta > \qquad \text{(B-14)}$$

where σ_i, σ_r are the lowest order expansions of

$$\sigma = \sigma_r + i\sigma_i = \sigma \int dX (1 - e^{i\eta}) . \qquad \text{(B-15)}$$

Anderson's theory[1] has an average over the perturber angular momentum, j_2

$$\sigma = \sum_{j_2} \rho_{j_2} \sigma_{j_2} \qquad \text{(B-16)}$$

where

$$\rho_{j_2} = (2j_2 + 1) \exp\left[-hcB_{j_2} (j_2 + 1)/kT\right] \Big/ \sum_{j_2} (2j_2 + 1) \exp\left[\frac{-hcB_{j_2} (j_2 + 1)}{kT}\right] \qquad \text{(B-16a)}$$

and

$$\sigma_{j_2} = \sigma \int dX \left[1 - \frac{1}{2j_2 + 1} \frac{Tr\mu_z^{if} T^{-1} \mu_z^{fi} T}{Tr\mu_z^{if} \mu_z^{fi}} \right] \tag{B-17}$$

where

$$\mu_z^{if} = \langle i | \mu_z | f \rangle \equiv \langle m | \mu_z | n \rangle \tag{B-18}$$

and

$(m|T|n)$ = S matrix element for transition from n to m, i.e. $|Smn|^2$ gives the probability of finding, at $t = +\infty$, the system in state m, if it was known to be in state n at $t = -\infty$. The trace term in the expression for σ_{j_2} has the form of a normalized autocorrelation function - i.e., it plays the role of the $e^{i\eta}$ factor.

C. METHODS OF EVALUATING THE ANDERSON RESULT

Use of the Wigner-Eckart theorem enables us to simplify Eq. (B-17)[5] so that, if b denotes the collision impact parameter

$$\sigma_{j_2} = \int db \; 2\pi b \; S_{j_2}(b) \tag{B-19}$$

where b denotes impact parameter and

$$S_{j_2}(b) = 1 - \sum_2 (j_f \; m_f \; 1 \; M | j_f \; 1 \; j_i \; m_i) (j_f \; m_f' \; 1 \; M | j_f \; 1 \; j_i \; m_i') \; x$$

$$\text{all } m \;\; x \; (j_f \; m_f \; j_2 \; m_2 | T^{-1}(b) | j_f \; m_f' \; j_2' \; m_2') \; (j_i \; m_i' \; j_2 \; m_2' \; x$$

$$x \; |T(b)| \; j_i \; m_i \; j_2 \; m_2). \tag{B-20}$$

In Eq.(B-20), j_i, j_f refer to the lower and upper states for the transition, a, m refer to the internal angular momentum and its component, and the sub-index 2 denotes the perturbing particle. Straight line trajectories are assumed and hence there is no need to specify the momentum states before and after the collision. Anderson,[1] as well as most of his followers,[5,6] have proceeded from Eq. (B-20) by expanding T in an infinite series.[7]

In practice, this is taken to be ($V_o \equiv \exp(i H_o t/\hbar)$)

$$T = 1 + \frac{1}{i\hbar}\int_{-\infty}^{\infty} V_o^{-1} H_c V_o \, dt + \frac{1}{(i\hbar)^2}\int V_o^{-1} H_c V_o \int_{-\infty}^{\infty} V_o^{-1} H_c(t') V \, dt\, dt$$

$$= 1 + \sum_n \frac{1}{(i\hbar)^n}\int V_o^{-1} H_c V_o(t_1) \ldots V_o^{-1} H_c V_o(t)\, \Theta(t_1 - t_2) \ldots \Theta(t_{n-1} - t_n)$$

$$dt_1 \ldots . dt_n \qquad \text{(B-21)}$$

Through second order, we have

$$S_2(b) = \frac{1}{2j_2+1}\left\{\sum_m \left[\frac{1}{2j_f+1}\,(j_f\, m_f\, j_2\, m_2 \left| T_1^{-1}(b) + T_2^{-1}(b) \right| j_f\, m_f\, j_2\, m_2)\right]\right.$$

$$+ \frac{1}{2j_i+1}\left[(j_i\, m_i\, j_2\, m_2 \left| T_1(b) + T_2(b) \right| j_i\, m_i\, j_2\, m_2)\right]$$

$$+ \frac{1}{2j_i+1}\,(j_f\, m_f\, 1\, M \left| j_f\, 1\, j_i\, m_i\right)(j_f\, 1\, m_f'\, M \;\; j_f\;\; j_i\, m_i') \times$$

$$\left. \times\, (j_f\, m_f\, j_2\, m_2 \left| T_1^{-1}(b) \right| j_f\, m_f'\, j_2'\, m_2')(j_i\, m_i'\, j_2\, m_2' \left| T_1(b) \right| j_i\, m_i\, j_2\, m_2)\right\}$$

(B-22)

where factors of the form ($j\; mj'\;\; m' \left|\; j\;\; j'\;\; j''\; m+m'$) denote the usual vector coupling coefficients.

$S_2(b)$ may be cast in a very useful form by means of Feynman graph techniques. The result is

$$S_2(b) \equiv \frac{1}{2j_2+1}\left[A_1(b) + A_{1\,\mathrm{eff}}(b) + A_2(b) + S_{2m}(b)\right] \qquad \text{(B-23)}$$

where, if

$$\tilde{H}_c(F) \equiv \int H_c(t) e^{iFt} dt \tag{B-23a}$$

$$A_1(b) = \frac{i}{(2j_f + 1)\hbar} \langle j_f\, m_f\, j_2\, m_2 \left| \tilde{H}_c(0) \right| j_f\, m_f\, j_2\, m_2 \rangle$$

$$+ \frac{i}{(2j_i + 1)\hbar} \langle j_i\, m_i\, j_2\, m_2 \left| \tilde{H}_c(0) \right| j_i\, m_i\, j_2\, m_2 \rangle, \tag{B-24}$$

$$A_{1_{eff}}(b) = -\frac{i}{(2j_f + 1)\hbar^2} \sum_{B_u} \int \left| (j_f\, m_f\, j_2\, m_2 | H_c(t) | B_u) \right|^2 dt/\omega_{fB_u} + \frac{i}{(2j_i + 1)\hbar^2} (i \leftrightarrow f) \tag{B-25}$$

(where B_u denotes the far lying intermediate states - i.e., those states for which the energy denominators $\omega_{fB_u} \equiv \omega_f + \omega_{j_2} - \omega_{B_u}$ and $\omega_{iB_u} = \omega_i + \omega_{j_2} - \omega_{B_u}$ are of the order of the vibrational spacing or higher), and

$$A_2(b) = \frac{1}{2j_f + 1} \cdot \frac{1}{2\hbar^2} \sum_{B_\ell} \left\{ \langle j_f\, m_f\, j_2\, m_2 \left| \tilde{H}_c(\omega_{fB_\ell}) \right| B_\ell \rangle^2 \right.$$

$$\left. - \frac{i}{\pi} P \int dF \frac{\left| \langle j_f\, m_f\, j_2\, m_2 \left| H_c(F) \right| B_\ell \rangle \right|^2}{\omega_{fB_\ell} - F} \right\}$$

$$+ (i \leftrightarrow f) \tag{B-26}$$

where B_ℓ denotes those states which yield energy denominators comparable to the molecular rotational spacings. $S_{2m}(b)$ denotes the last term of Eq. (23) which we have not explicitly simplified.

The prime advantage of Eq. (26) is that the real part of A_2, which contributes to the line broadening, has already been explicitly evaluated for a wide range of interactions.[5, 8] The imaginary part of A_2, which is a shift contribution, involves the same matrix elements! We need only perform an additional Hilbert transform to obtain the imaginary part of $A_2(b)$. We illustrate this explicitly for a dipole-dipole interaction.

Tsao and Curnutte[5] give, for a dipole-dipole interaction, the following result:

$$S_{2REAL} = \frac{4}{9}\left(\frac{p_1 p_2}{hv}\right)^2 \sum (j_i\ 0\,|0|\,j_i|\,j_i'\ 0)^2\ (j_2\ 0\,|0|\,j_2|\,j_2'\ 0)^2\ f_1(|k|)$$

$$+ (i \leftrightarrow f) \qquad \text{(B-27)}$$

where p is the dipole moment, k in the initial state is $\left[\omega_{j_i'} + \omega_{j_2'} - \omega_{j_i} - \omega_{j_2}\right] b/v$, and $f_1(|k|)$ is a tabulated function, expressible as a bilinear sum of modified Hankel functions. For example, for a fixed j_i and j_2, consider the intermediate state $j_i - 1$, $j_2 + 1$. Then

$$k = \frac{2\pi B_r b}{v/c}\left[j_i(j_i+1) - (j_i+1)(j_i+2)\right]$$

$$+ \frac{2\pi B_p b}{v/c}\left[j_2(j_2+1) - j_2(j_2-1)\right]$$

$$= \frac{2\pi b}{v/c}\left[-2B_r(j_i+1) + 2B_p j_2\right] \qquad \text{(B-28)}$$

where B_r, B_p denote the rotational constants of the radiator and perturber in the initial state. In shift calculations we may use this formalism intact, pausing only to take the Hilbert transform of f(k). That is, in place of $f_1(k)$ we use

$$g_1(k) = \frac{1}{\pi} P \int dx \frac{f_1(x)}{k - x} \qquad \text{(B-29)}$$

then, if dipole-dipole were the only interaction, we would have[5] for a particular value of j_1

$$(\Delta\nu)_{\substack{\text{shift in} \\ \text{cm}^{-1}}} = - \frac{nv}{2\pi c} \operatorname{Im} \sigma(j_1). \qquad \text{(B-30)}$$

Calculations were performed using Eqs. (30) and (31) and the following interactions through b^{-8}

(a) dipole-dipole

(b) dipole-quadrupole

(c) quadrupole-dipole

(d) quadrupole-quadrupole

(e) effective first order interaction
(induction and dispersion)

The quadrupole-quadrupole contributes in first order as well as second. All the others possess second order interactions only, since the expectation value of the dipole moment components is zero for interactions (a) - (c). Therefore, we may take the results of Tsao and Curnutte, pausing only to replace each f(k) function by its Hilbert transform. For the quadrupole-quadrupole, we have treated the second order term in this fashion, and have explicitly evaluated the first order term as well as the effective first order (dispersion) interaction.

Equations (30) and (31), as they stand, are insufficient to calculate the desired line shifts. The reason for this is that $S_2(b)$ diverges as $b \to 0$ as does $\sigma(j_1)$. A cutoff is necessary, and we turn our attention now to an analysis of this question.

D. THE CUTOFF

Clearly, the cutoff procedure must become operative at value of b (the impact parameter) where the expansion, Eq. (21), ceases to be valid. For a dipole-dipole interaction the expansion parameter is of the order of ($P \equiv$ dipole moment 10^{-18} e. s. u. cm $\equiv eb_o$)

$$\left[\frac{1}{\hbar}\int H_c(t)\,dt\right] \sim \frac{P^2}{\hbar b^3} \cdot \frac{b}{v} = \frac{1/137}{v/c}\,\frac{b_o^2}{b^2} \qquad \text{(B-31)}$$

Typically this parameter approaches one when

$$D < 12\ \text{Å} \qquad \text{(B-32)}$$

which is triple the typical collision diameter. Several ad-hoc cutoff procedures were advanced by Anderson[1] for line broadening problems. For line shift calculations, Sharma and Caledonia proceeded as follows. Physically, S(b) cannot exceed unity as may be seen from its definition, Eqs. (19) and (20). Accordingly, Sharma and Caledonia multiply Im S(b) for each j_2 by factor 1-ReS(b), with the added proviso that the integration over the impact parameter b vanish for ReS(b) > 1. This procedure has several advantages:

a) It is convenient - since the cutoff is not m dependent, sums over magnetic quantum numbers may be taken and the unitarity of the appropriate vector coupling coefficients utilized.

b) It cuts off for small b.

The nature of this cutoff is very rough, however. Mainly because of the first property, and our desire to use the results of Tsao and Curnutte, we have utilized the Sharma - Caledonia procedure. The true villain of the piece, however, is the utilization of the expansion Eq. (21). A far more efficient expansion of the matrix element $(m|T|n)$ has been given by Murphy and Boggs[9] in the course of constructing an alternative theory for line shift and broadening. A close reading of this work, however, indicates that their principal contribution has been their alternative to the expansion Eq. (21), rather than their alternative to Anderson's Equation, Eq. (17). The Murphy-Boggs expansion, which puts the expansion in a negative exponential, has the great advantage that $S_2(b) \to 0$ (both real and imaginary parts) without the need for any artificial cutoff. Its great disadvantage is that it is m dependent, ensuring the necessity for a long machine calculation.

One final point. In utilizing a cutoff with a $1-\text{Re}S_2(b)$ factor, the last term in Eq. (22), the so-called S_2 middle term is omitted. The physical reason for this is that it yields a better approximation to the true (Murphy-Boggs) cutoff.

E. THE RESULTS

As a check on the procedure we have used, we calculated the $0 \to 2$ vibration-rotation shifts for DCl perturbed by HCl and for HCl perturbed

by DCl at a temperature of 300°K. The results of our calculations are given in Figs. 9 and 10, where the results of Sharma and Caledonia have been given for comparison. It appears that our predictions are closer to the observed values than those of Sharma and Caledonia except at high j_1 values in the R bands where they are worse.

The results for the 0 → 2 CO band perturbed by N_2 are given in Fig. 11. For comparison, the measured CO-A shifts are also presented. It is seen that the two sets are comparable.

F. ANALYSIS OF THE RESULTS

We note that the DCl-HCl shifts exhibit an oscillation with j. Jaffe, et al.[4] explained this in terms of an alternating rotational-resonance, but noted that the wrong sign was obtained. A detailed analysis shows that this is not surprising. The rotational-resonance gives, in fact, a zero contribution to the line shift. Hence, rather than the rotational-resonance intermediate state dominating the shift, it constitutes a "hole", leading to an opposite sign than that predicted by Jaffe.

In our calculations we have neglected the dipole-octopole and octopole-dipole interactions included by Sharma and Caledonia. However, it was found that the second order quadrupole-quadrupole interaction, which is of the same order as the dipole-octopole and octopole-dipole, contributed only several percent to the final results. Also, we expect little contribution from these in the CO-N_2 interaction, the dipole moments of CO and N_2 being $(.12) \times 10^{-18}$ esu-cm and zero respectively.

Finally, we note that our results do not match experiment well at high j values. Physically, the reasons for this is as follows. At high j values, the energy denominators in Eq. (26) increase, for a fixed value of b. In this region, however, the whole analysis is open to question, due to the expansion used, Eq. (21). Hopefully, a careful application of the Murphy-Boggs cutoff will yield results for high j levels which are more in accord with experiments.

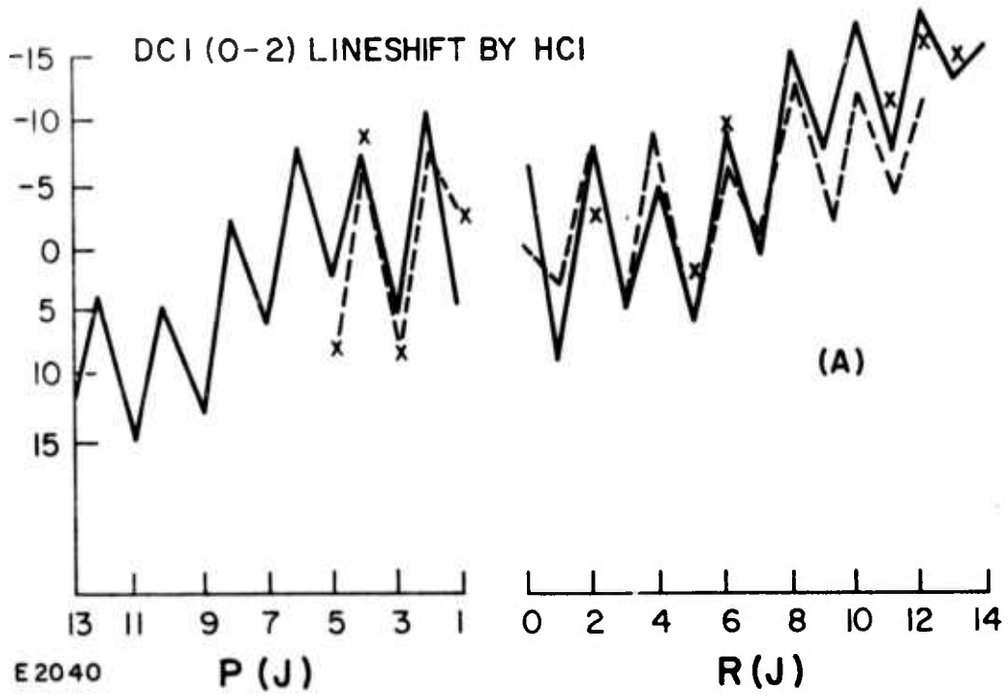

Fig. 9 Shift of DCℓ 0 → 2 band by HCℓ per atmosphere HCℓ. Units are 1.0×10^{-3} cm^{-1}. Crosses represent experimental points (Ref. 4). Solid line is the calculation of Ref. 3. The hatched line is the present report.

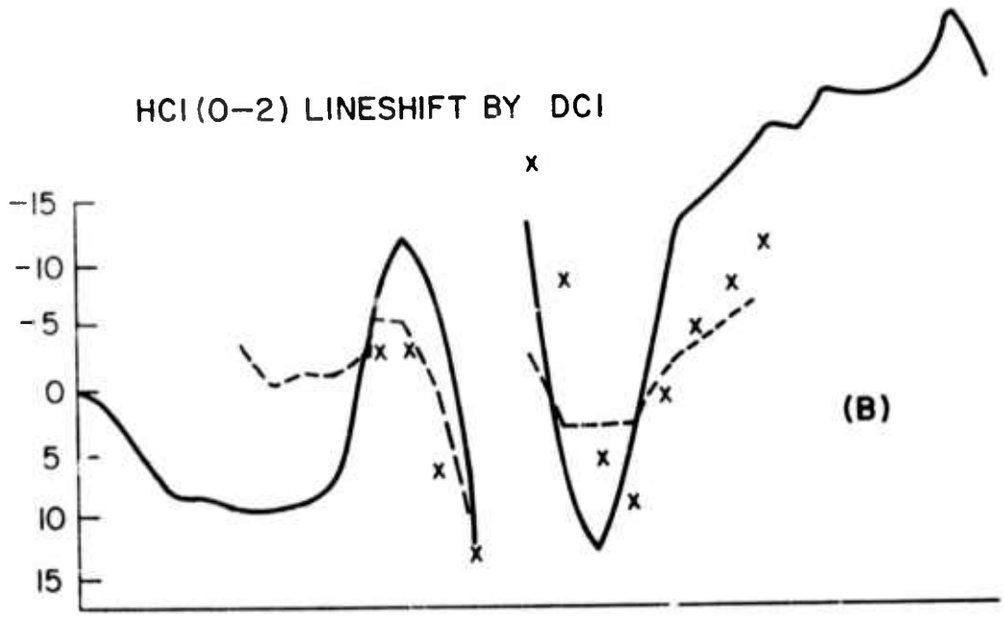

Fig. 10 Shift of HCℓ 0 → 2 band by DCℓ per atmosphere DCℓ. Units are 1.0×10^{-3} cm^{-1}. Crosses represent experimental points (Ref. 4). Solid line is the calculation of Ref. 3. The hatched line is the present report.

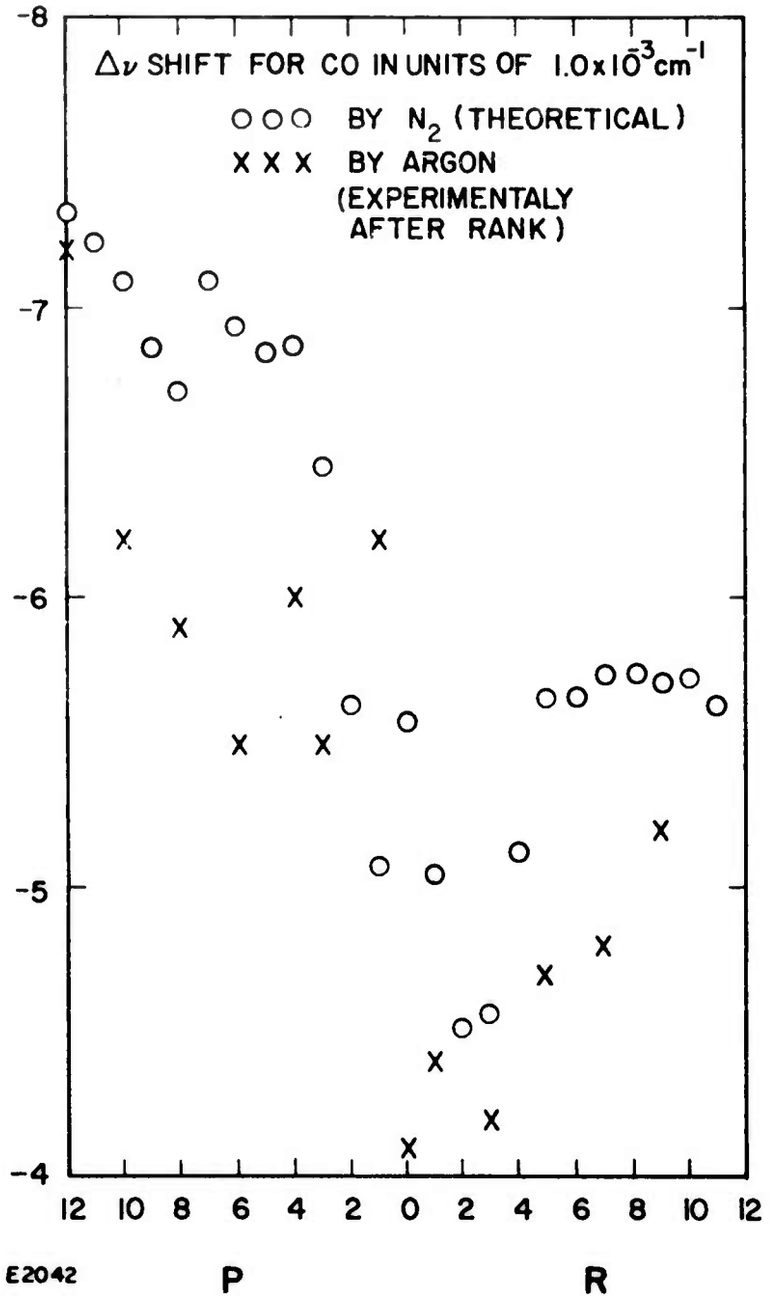

Fig. 11 Shift of CO 0 → 2 band by N_2 per atmosphere N_2 (crosses). The experimental shifts due to Argon (dots) are presented for comparison (c.f. Ref. 2).

APPENDIX B

REFERENCES

1. P. W. Anderson, PR 76, #5, 647 (1949).

2. C. Boulet, P. Isnard, and A. Levy, JQRST, 13, 911 (1973).

3. R. D. Sharma and G. Caledonia, J. Chem. Phys., 54, 434 (1971).

4. J. H. Jaffe, M. A. Hirshfeld, and A. Ben Reuven, J. Chem. Phys., 40, 1705 (1963).

5. C. J. Tsao and B. Curnutte, JQRST, 2, 41 (1962).

6. A. Ben Reuven, H. Friedmann, and J. H. Jaffe, J. Chem. Phys., 38, 3021 (1963).

7. A. S. Davydov, Quantum Mechanics, Eq. 74.12, Pergamon Press, New York (1965).

8. D. Robert, M. Giraud, and L. Galatry, J. Chem. Phys., 51, #5, 2192 (1969).